

Evidence for the First Excited State of ${}^7\text{H}$

A. A. Bezbakh,^{1,2} V. Chudoba,^{1,2,*} S. A. Krupko,^{1,3} S. G. Belogurov,^{1,4} D. Biare,¹ A. S. Fomichev,^{1,5} E. M. Gazeeva,¹ A. V. Gorshkov,¹ L. V. Grigorenko,^{1,4,6} G. Kaminski,^{1,7} O. A. Kiselev,⁸ D. A. Kostyleva,^{8,9} M. Yu. Kozlov,¹⁰ B. Mauey,^{1,11} I. Mukha,⁸ I. A. Muzalevskii,^{1,2} E. Yu. Nikolskii,^{6,1} Yu. L. Parfenova,¹ W. Piatek,^{1,7} A. M. Quynh,^{1,12} V. N. Schetinina,¹⁰ A. Serikov,¹ S. I. Sidorchuk,¹ P. G. Sharov,^{1,2} R. S. Slepnev,¹ S. V. Stepanov,¹ A. Swiercz,^{1,13} P. Szymkiewicz,^{1,13}

G. M. Ter-Akopian,^{1,5} R. Wolski,^{1,14} B. Zalewski,^{1,7} and M. V. Zhukov¹⁵

¹Flerov Laboratory of Nuclear Reactions, JINR, 141980 Dubna, Russia

²Institute of Physics, Silesian University in Opava, 74601 Opava, Czech Republic

³SSC RF ITEP of NRC “Kurchatov Institute,” 117218 Moscow, Russia

⁴National Research Nuclear University “MEPhI,” 115409 Moscow, Russia

⁵Dubna State University, 141982 Dubna, Russia

⁶National Research Centre “Kurchatov Institute,” Kurchatov sq. 1, 123182 Moscow, Russia

⁷Heavy Ion Laboratory, University of Warsaw, 02-093 Warsaw, Poland

⁸GSI Helmholtzzentrum für Schwerionenforschung GmbH, 64291 Darmstadt, Germany

⁹II. Physikalisches Institut, Justus-Liebig-Universität, 35392 Giessen, Germany

¹⁰Laboratory of Information Technologies, JINR, 141980 Dubna, Russia

¹¹Institute of Nuclear Physics, 050032 Almaty, Kazakhstan

¹²Nuclear Research Institute, 670000 Dalat, Vietnam

¹³AGH University of Science and Technology, Faculty of Physics and Applied Computer Science, 30-059 Krakow, Poland

¹⁴Institute of Nuclear Physics PAN, Radzikowskiego 152, 31342 Kraków, Poland

¹⁵Department of Physics, Chalmers University of Technology, S-41296 Göteborg, Sweden



(Received 25 June 2019; revised manuscript received 13 September 2019; published 16 January 2020)

The ${}^7\text{H}$ system was populated in the ${}^2\text{H}({}^8\text{He}, {}^3\text{He}){}^7\text{H}$ reaction with a 26 A MeV ${}^8\text{He}$ beam. The ${}^7\text{H}$ missing mass energy spectrum, the ${}^3\text{H}$ energy and angular distributions in the ${}^7\text{H}$ decay frame were reconstructed. The ${}^7\text{H}$ missing mass spectrum shows a peak, which can be interpreted either as unresolved $5/2^+$ and $3/2^+$ doublet or one of these states at 6.5(5) MeV. The data also provide indications of the $1/2^+$ ground state of ${}^7\text{H}$ located at 1.8(5) MeV with quite a low population cross section of $\sim 25 \mu\text{b}/\text{sr}$ within angular range $\theta_{\text{c.m.}} \simeq (17^\circ - 27^\circ)$.

DOI: 10.1103/PhysRevLett.124.022502

Introduction.—The ${}^7\text{H}$ nucleus is the heaviest conceivable hydrogen isotope with the largest $A/Z = 7$ ratio. The ${}^7\text{H}$ ground state (g.s.) decays via the unique five-body ${}^3\text{H} + 4n$ channel. Corresponding decay dynamics is not yet studied and it can lead to such an exclusive phenomenon as $4n$ radioactivity [1,2]. There were very few theoretical predictions for the ${}^7\text{H}$ g.s. energies. The hyperspherical harmonics model [3] evaluated it as $E_T \approx 3$ MeV (E_T is energy relative the ${}^3\text{H} + 4n$ threshold). The phenomenological studies in [1] pointed to $E_T \sim 1.3$ – 1.8 MeV. The antisymmetrized molecular dynamics [4] provided $E_T = 4.2$ MeV. No predictions for the ${}^7\text{H}$ excited states were ever made.

The ${}^7\text{H}$ nucleus was searched unsuccessfully among the ternary fission products of ${}^{252}\text{Cf}$ [5] and in the ${}^7\text{Li}(\pi^-, \pi^+)$ reaction [6]. The radioactive ion beams offer a natural way to search for ${}^7\text{H}$ using the proton removal from ${}^8\text{He}$. The ${}^1\text{H}({}^8\text{He}, {}^2\text{He})$ reaction was used in Ref. [7] and evidence for the population of the ${}^7\text{H}$ spectrum right above the ${}^3\text{H} + 4n$ threshold was demonstrated. The search for a long-living

(hence small E_T) ${}^7\text{H}$ produced in the ${}^2\text{H}({}^8\text{He}, {}^3\text{He})$ reaction was made in Ref. [1] resulting in the ascertainment of the lower decay-energy limit $E_T > 50$ – 100 keV for the ${}^7\text{H}$ g.s. The observation of a low-lying ${}^7\text{H}$ resonant state populated in the ${}^{12}\text{C}({}^8\text{He}, {}^7\text{H}){}^{13}\text{N}$ reaction was declared in [8]. Inherent to this work was the difficulty of the reaction-channel identification. The next attempt to discover ${}^7\text{H}$ was made using the ${}^2\text{H}({}^8\text{He}, {}^3\text{He})$ reaction [9]. A smooth missing mass (MM) spectrum was obtained, but the authors pointed out a peculiarity at $E_T \sim 2$ MeV with cross section $\sim 30 \mu\text{b}/\text{sr}$.

Though the ${}^7\text{H}$ production from ${}^8\text{He}$ seems to be a straightforward idea, it had not provided a decisive result so far. In the present Letter, we have obtained for the first time a reliable quantitative result for the ${}^7\text{H}$ energy spectrum coming closer to the solution of the ${}^7\text{H}$ g.s. problem.

Experiment.—The work was performed at the Flerov Laboratory of Nuclear Reactions (JINR) at the ACCULINNA-2 fragment separator [10]. The 33.4 A MeV primary ${}^{11}\text{B}$ beam was delivered by the U-400M cyclotron with the intensity of $\sim 1 \mu\text{A}$. It was focused into a 5-mm spot

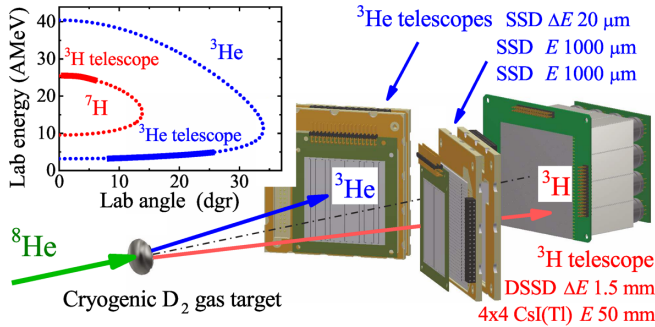


FIG. 1. The experimental setup. The inset presents kinematical conditions of the ${}^2\text{H}({}^8\text{He}, {}^3\text{He}){}^7\text{H}$ reaction at 26 AMeV. The solid lines correspond to the kinematical area which is accessible by the used setup.

on the 1-mm thick beryllium production target. The secondary ${}^8\text{He}$ beam with energy 26 AMeV, $\sim 90\%$ purity, and intensity $\sim 10^5$ pps, was focused into a 17-mm spot on the deuterium gas target. The 4 mm thick gas cell was equipped with $6\ \mu\text{m}$ stainless steel windows. The D_2 target was cooled to 27 K, and its thickness made $\sim 3.8 \times 10^{20}\ \text{cm}^{-2}$. The secondary beam diagnostics was performed by the two multiwire proportional chambers and the pair of thin plastics [11].

The experimental setup is shown in Fig. 1. The two identical $\Delta E - E - E$ telescopes were destined to detect the 9–30 MeV ${}^3\text{He}$ nuclei emitted in the ${}^2\text{H}({}^8\text{He}, {}^3\text{He}){}^7\text{H}$ reaction. Each telescope consisted of three Si detectors: one 20-micron SSD ($50 \times 50\ \text{mm}^2$, 16 strips) and two 1000-micron SSDs ($61 \times 61\ \text{mm}^2$, 16 strips). The telescopes were located 166 mm downstream from the D_2 target covering an angular range of $\sim (8^\circ - 26^\circ)$ in laboratory system. Tritons emitted from ${}^7\text{H}$ were detected by the $64 \times 64\ \text{mm}^2$ telescope installed at zero laboratory angle 280 mm downstream from the target. It consisted of one 1500-micron Si DSD (32×32 strips) and a set of 16 square CsI(Tl)/PMT modules.

For the ${}^3\text{He}$ recoils detected in coincidence with ${}^3\text{H}$, the MM value was reconstructed assuming that the reaction occurred in the middle plane of the target. This is the main limiting factor defining the 1.1 MeV (FWHM) resolution of the ${}^7\text{H}$ MM measurement.

Missing mass spectrum.—The number of ${}^3\text{He}$ - ${}^3\text{H}$ coincidences found in the recorded data was 113 including 105 events identified as the population of ${}^7\text{H}$. Figure 2(a) shows the correlation plot between the ${}^7\text{H}$ MM and ${}^3\text{H}$ energy in the ${}^7\text{H}$ center-of-mass (c.m.) frame. It can be seen that the majority of data is in agreement with the hypothesis of the ${}^7\text{H}$ population and its subsequent decay with emission of ${}^3\text{H}$. The experimental data acquired with the empty target showed that the contribution of the background, made by the reactions on the target windows, was at a level of 10%. The MM spectrum of ${}^7\text{H}$ is shown in Figs. 2(b) and 2(c) in different representations. In this spectrum, the peak with

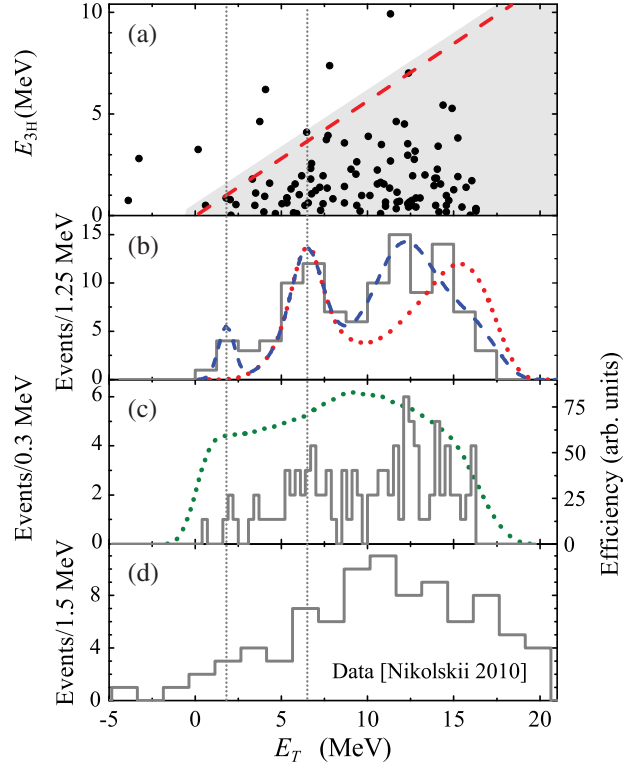


FIG. 2. (a) Correlation between the ${}^3\text{H}$ energy in the ${}^7\text{H}$ c.m. frame and the ${}^7\text{H}$ MM energy. Red dashed line shows the kinematical limit for tritons coming from the ${}^7\text{H}$ decay. Grey triangle represents kinematically allowed region used for the reconstruction of the MM spectrum. Panels (b) and (c) show the ${}^7\text{H}$ MM spectrum shown with two different binning factors. The red dotted curve in (b) shows the fit to the data by the 6.5 MeV resonant state with $\Gamma = 2$ MeV plus the contribution of the $t + 4n$ five-body phase space. The blue dashed curve shows the fit with the addition of the 1.8 MeV ($\Gamma < 300$ keV) and 12 MeV ($\Gamma = 4$ MeV) resonances. The both curves were convoluted with the setup efficiency [green dotted curve in panel (c)] and MM resolution. (d) The data from Ref. [9]. Vertical dotted lines indicate the presumed positions of the ${}^7\text{H}$ ground and first excited states.

energy $E_T = 6.5(5)$ MeV, width $\Gamma = 2.0(5)$ MeV, is identified. For the description of this peak, see the dashed and dotted curves in Fig. 2(b), we used the Lorentzian profile with the energy-dependent $\Gamma(E_T)$ [2]. The standard χ^2 tests of the hypotheses provided in Fig. 2(b) give confidence level 0.9–0.95 for the 6.5 MeV peak within the energy interval $3 < E_T < 11$ MeV. In contrast, the assumption that this spectrum can be described by some smooth distribution gives confidence level 0.05–0.25 depending on details. So, we conclude with a good reason the presence of the 6.5 MeV resonance in the measured MM spectrum of ${}^7\text{H}$. We interpret this peak as the first excited state of ${}^7\text{H}$, though we cannot exclude the population of the $5/2^+$ and $3/2^+$ doublet of the lowest excited states. For the 6.5 MeV resonance, represented by 27 events in $5 < E_T < 8$ MeV

interval, the average cross section estimate $\sim 30 \mu\text{b}/\text{sr}$ was obtained for the $10^\circ\text{--}45^\circ$ c.m. angular range.

A compact group of events at $E_T \sim 1.8 \text{ MeV}$ is also present in the MM spectrum shown in Figs. 2(b) and 2(c). This group can be associated with the population of the ${}^7\text{H}$ g.s. with the cross section of $\sim 25 \mu\text{b}/\text{sr}$ in the $17^\circ\text{--}27^\circ$ c.m. angular range. Such an interpretation is at the limit of statistical significance and deserves special discussion.

The spectrum rise at $E_T > 10 \text{ MeV}$ can be well fitted by a resonance contribution at $E_T = 12 \text{ MeV}$ with $\Gamma = 4 \text{ MeV}$, see blue dashed curve in Fig. 2(b). However, idea about another resonance at 12 MeV should be considered with caution: the MM spectrum at $E_T > 10 \text{ MeV}$ can also be explained by the combination of a rapidly growing five-body phase space and rapidly falling detection efficiency, see the red dotted curve in Fig. 2(b).

Reaction cross section calculations.—The FRESKO code [12] was employed in the calculations of the ${}^2\text{H}({}^8\text{He}, {}^3\text{He}){}^7\text{H}$ reaction. The ${}^7\text{H}$ g.s. population was assumed to be one-step proton transfer from the bare ${}^4\text{He}$ core of ${}^8\text{He}$. The Woods-Saxon potentials with diffuseness 0.55 fm and radii $r = r_0 A^{1/3}$ were adopted, where $r_0 = 1.45 \text{ fm}$ for ${}^7\text{H}$ and $r_0 = 1.3 \text{ fm}$ for ${}^2\text{H}$ channels. The potential strengths were adjusted to match the proton binding energies in ${}^8\text{He}$ and ${}^3\text{He}$. Following Ref. [13], the spectroscopic factor (SF) $3/2$ for the ${}^3\text{He} \rightarrow d + p$ vertex was taken. For the ${}^8\text{He} \rightarrow {}^7\text{H} + p$ the SF value of 2 was taken (assumed to be the same as for the ${}^4\text{He} \rightarrow {}^3\text{H} + p$ vertex). The entrance-channel (${}^8\text{He} + d$) and the exit-channel (${}^7\text{H} + {}^3\text{He}$) optical model (OM) parameters were obtained based on Refs. [14,15].

The calculated differential cross section for the population of the ${}^7\text{H}$ $1/2^+$ g.s. in the one-step ${}^2\text{H}({}^8\text{He}, {}^3\text{He}){}^7\text{H}$ reaction is shown in Fig. 4(a). When the potential radius parameters r_0 are varied within 10%, the position of the first diffraction minimum is varied within $\sim 1^\circ$. A similar $\sim 1.5^\circ$ variation of this minimum was obtained employing the OM parameters borrowed from ${}^9\text{Be} + {}^3\text{He}$ system at 31.6 MeV from compilation [16]. This variation of the inputs did not result in an appreciable change of the second diffraction maximum position. However, the cross section value for the second maximum was found to be sensitive to the adopted ${}^7\text{H}$ decay energy. Overall, the cross section profile predicted for the ${}^7\text{H}$ g.s. appears to be quite stable.

The calculations for the ${}^7\text{H}$ $3/2^+$ and $5/2^+$ excited states are shown in Fig. 4(b). The population of these states goes via the proton transfer from the ${}^8\text{He}(2^+)$ state appearing due to the collective excitation with $\beta_2 = 0.45$.

Discussion of the ${}^7\text{H}$ ground state evidence.—We consider the group of five events within $0.5 < E_T < 2.5 \text{ MeV}$ range as candidates for the ${}^7\text{H}$ g.s. Here, we discuss several arguments supporting this notion. (i) Figure 3 demonstrates the good quality of the ${}^3\text{He}$ recoil identification. It is clear that the ${}^3\text{He}$ identification in the zero-angle telescope is essentially better. Thus the identification of the ${}^7\text{H}$ decay

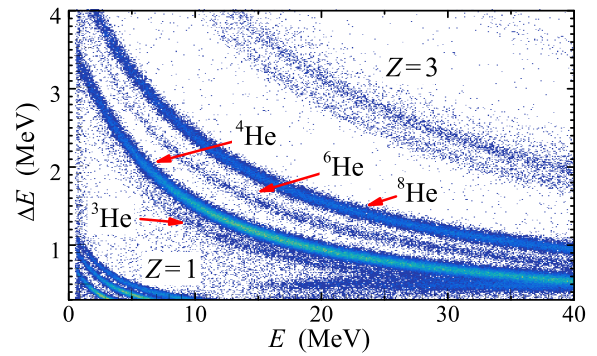


FIG. 3. The ${}^3\text{He}$ recoil identification.

channel is unambiguous for all the events in Figs. 2(b) and 2(c). (ii) The c.m. angles of the ${}^7\text{H}$ g.s. candidate events are shown by arrows in Fig. 4(a). It can be seen that all events are concentrated in the region predicted to be the second diffraction maximum for the calculated cross section of the $1/2^+$ state. In principle, one might expect the detection of a similar number of the g.s. events in the range of $6^\circ < \theta_{\text{c.m.}} < 12^\circ$. However, we do not think that the nonobservation of events in this region is an important fact. The position of the first cross section minimum varies within 1.5° in our calculations. Somewhat larger shift of the minimum towards smaller angles is not impossible and, together with the sharp efficiency cutoff, it can provide the explanation. The deduced average cross section value of $25 \mu\text{b}/\text{sr}$ for the c.m. angular range $17^\circ\text{--}27^\circ$ should be compared with the average calculated values $\sim 400\text{--}600 \mu\text{b}/\text{sr}$, implying quite a low experimental SF $\sim 0.08\text{--}0.12$ for the ${}^7\text{H}$ vertex. (iii) Among the five-body correlations predicted for the ${}^7\text{H}$ decay in the recent paper [17], only the energy distribution of ${}^3\text{H}$ in the ${}^7\text{H}$ frame can be reconstructed from our data. For this distribution quite a narrow low-energy peak is predicted, which can be affected by the decay dynamics of ${}^7\text{H}$. Due to its lowest possible five-body centrifugal barrier, the $[s_{1/2}^2 p_{3/2}^2]_0$ configuration is expected to dominate the decay of the ${}^7\text{H}$ g.s. The comparison of the corresponding calculations from [17] with the experimental data is presented in Fig. 5(a). We also calculated the angular distributions of the ${}^3\text{H}$ emission relative to the retrieved ${}^7\text{H}$ flight direction in the laboratory frame, see Fig. 5(b). In contrast to the ${}^3\text{H}$ energy, measured with accuracy $\sim 2\%$, the emission angle is reconstructed with higher precision: the ${}^3\text{H}$ direction is determined with resolution of 0.5° by the central telescope, and the ${}^7\text{H}$ direction is derived with a precision of 0.5° . All the candidate g.s. events well fit the distribution curves predicted for the ${}^7\text{H}$ g.s. $E_T = 2 \text{ MeV}$. And (iv) we made the statistical analysis for the 5 ${}^7\text{H}$ g.s. candidate events within the maximum likelihood method appropriate for the low-statistics data. The Monte Carlo generated likelihood functions (recalculated in terms of confidence level) are shown in Fig. 5(c).

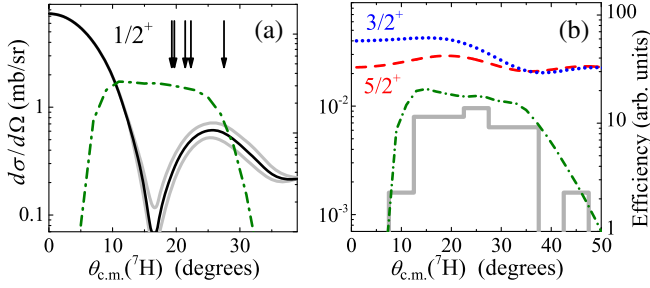


FIG. 4. The c.m. angular distributions calculated for the ${}^2\text{H}({}^8\text{He}, {}^3\text{He}){}^7\text{H}$ reaction channels. The angles of the five ${}^7\text{H}$ g.s. candidate events are indicated by arrows in (a). The gray curves in (a) show the $1/2^+$ cross section for ± 300 keV variation of the ${}^7\text{H}$ g.s. energy. The gray histogram in (b) shows (in arbitrary units) the experimental angular distribution in the $E_T = 5$ –8 MeV range (27 events). The green dash-dotted curves, associated with the arbitrary-scale right axes, show the setup efficiency for the registration of ${}^7\text{H}$ with $E_T = 1.8$ MeV and $E_T = 6.5$ MeV, respectively.

The 1.8 MeV decay energy with the 0.5 MeV uncertainty at the 1σ level can be safely inferred from the MM information (Fig. 2) and from the angular distribution of Fig. 5(b). The confidence interval found in Fig. 5(c) from the energy distribution of Fig. 5(a) is much broader and is also shifted (probably due to the underestimated energy resolution in our simulations). Nevertheless, it is consistent with the above g.s. energy prescription at a 1σ level. It should be noted that the three types of consistency checks for the ${}^7\text{H}$ g.s. candidate events provided in Fig. 5(c) are mutually independent from the experimental viewpoint (MM comes from the ${}^3\text{He}$ momenta reconstruction in the side telescopes, $E_{3\text{H}}$ depends on the ${}^3\text{H}$ energy resolution, and $\theta_{3\text{H}-7\text{H}}$ depends on the ${}^3\text{H}$ angular resolution given by the central telescope only). This is an encouraging fact supporting our interpretation of the data.

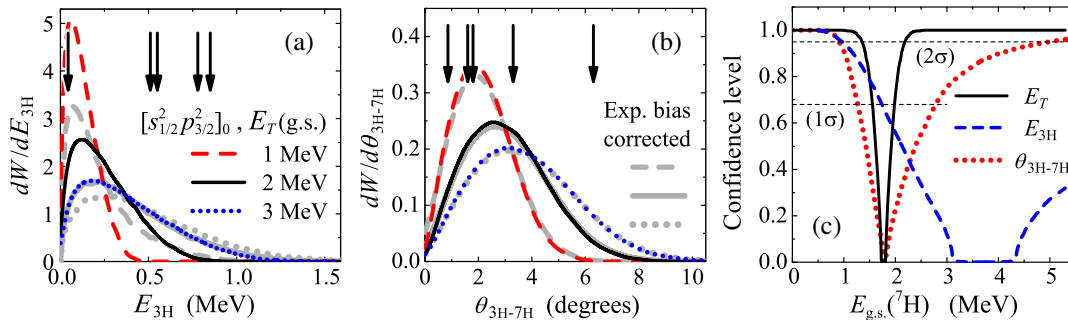


FIG. 5. (a) Energy distribution of tritons (in the ${}^7\text{H}$ frame) from the ${}^7\text{H}$ g.s. decay. (b) Distribution of angles between triton and ${}^7\text{H}$ in the laboratory frame. The colored curves in (a) and (b) are predicted for the different ${}^7\text{H}$ g.s. decay energies, while the gray curves of the corresponding style show the distributions corrected for the experimental resolution. The energies and angles of the five ${}^7\text{H}$ g.s. candidate events are indicated by arrows. Panel (c) shows the likelihood functions for the ${}^7\text{H}$ g.s. energy deduced from Fig. 2 (black solid curve), ${}^3\text{H}$ energy distribution from panel (a) (blue dashed curve), and ${}^3\text{H}$ angular distribution from panel (b) (red dotted curve). The intersections of these functions with the horizontal dashed lines at 0.68 and 0.95 define the confidence intervals for 1σ and 2σ levels, respectively.

Thus, the ${}^7\text{H}$ g.s. position at $E_T = 1.8(5)$ MeV is suggested in the present Letter. This value is consistent with the observation of a near-threshold anomaly in [7]. Our spectrum of ${}^7\text{H}$ for $E_T < 8$ MeV is consistent with the spectrum of Ref. [9], see Fig. 2(d). The latter was obtained in the same reaction at different energy but with worse energy resolution. The g.s. energy value inferred for ${}^7\text{H}$ in the present work does not differ radically from the value $E_T = 0.57^{+0.42}_{-0.21}$ MeV reported in Ref. [8]. Among the theoretical results, mentioned in the introduction, there is a good agreement with the phenomenological predictions of [1]: $E_T \sim 1.3$ –1.8 MeV.

Discussion of the ${}^7\text{H}$ excited state.—Figure 4(b) shows that the angular distribution for the events associated with the 6.5 MeV resonance is reasonably consistent with the distribution calculated for the $5/2^+$ and $3/2^+$ states (taking into account the setup efficiency). Also, if one compares the obtained $30 \mu\text{b/sr}$ average cross section value for the 10° – 45° c.m. angular range, the SF for ${}^7\text{H}^*$ population can be estimated as ~ 1 .

The ${}^7\text{H}$ has the closed $p_{3/2}$ neutron subshell. Systems with the shell closure typically have quite poor low-lying excitation spectra (see, e.g., [18]), and the easiest expectation is that the lowest is the 2^+ state formed by pushing neutrons to the $[p_{3/2}^2 p_{1/2}^2]_2$ configuration. This should be coupled with the core spin to the $5/2^+ - 3/2^+$ doublet. However, the separation of the doublet members is questionable, and here we can refer only to the experience of the ${}^5\text{H}$ excited states' studies [19], where this separation was found to be insignificant.

The systematics of the lowest excited states obtained for the light nuclei with the closed $p_{3/2}$ neutron orbital is given in Fig. 6. It can be seen that the states which can be related to the excitations of the neutron configurations have excitation energies $E^* \sim 3.0$ –4.5 MeV. In this plot the ${}^7\text{H}$ excitation energy is determined assuming that the group

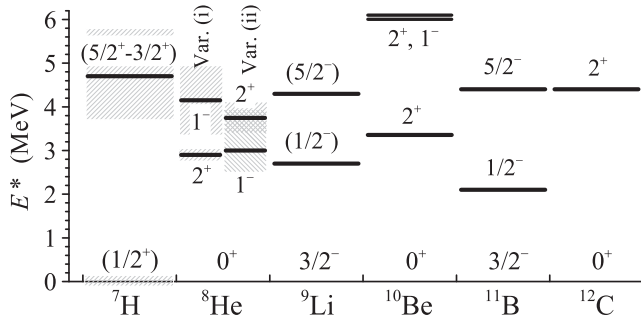


FIG. 6. Systematics of the lowest excited states for the isotones with closed $p_{3/2}$ neutron subshell. There exist two different prescriptions for the low-lying ${}^8\text{He}$ spectrum: (i) 2^+ , 1^- [20,21] and (ii) 1^- , 2^+ [22].

of events at $E_T \sim 1.8$ MeV represents the g.s. This gives the energy $E^* \sim 4.7$ MeV for the ${}^7\text{H}$ excited state, fitting well the systematics. If we assume a lower g.s. E_T value (e.g., $E_T < 1$ MeV), then we get unexpectedly high energy for the ${}^7\text{H}$ excited state, $E^* > 5.5$ MeV. This can be considered as an additional argument supporting our prescription made for the ${}^7\text{H}$ g.s.

Conclusion.—The following major results are obtained in this work. (i) For the first time, the ${}^7\text{H}$ excited state is observed at $E_T = 6.5(5)$ MeV with $\Gamma = 2.0(5)$ MeV. This state can be interpreted as the unresolved $5/2^+$ and $3/2^+$ doublet built upon the 2^+ excitation of valence neutrons, or one of the doublet states. (ii) Indications for the ${}^7\text{H}$ g.s. at $E_T = 1.8(5)$ MeV are found in the measured energy and angular distributions. The cross section obtained for the presumed ${}^7\text{H}$ g.s. populated in the ${}^8\text{He}(d, {}^3\text{He}){}^7\text{H}$ reaction in the c.m. angular range $17^\circ - 27^\circ$ is about $25 \mu\text{b}/\text{sr}$. This corresponds to a weak population of the g.s. with experimental SF ~ 0.1 , which clarifies why the previous searches for the ${}^7\text{H}$ g.s. required so much time and efforts without bringing reliable assignments of such a remote isotope.

The obtained results represent an important step towards resolving the problem of the ${}^7\text{H}$ observation.

We acknowledge important contribution of Professor M. S. Golovkov to the development of the experimental setup. This work was supported in part by the Russian Science Foundation Grant No. 17-12-01367 and Ministry of Education, Youth and Sports, Czech Republic (Project No. LTT17003).

* chudoba@jinr.ru

[1] M. S. Golovkov, L. V. Grigorenko, A. S. Fomichev, Y. T. Oganessian, Y. I. Orlov, A. M. Rodin, S. I. Sidorchuk, R. S. Slepnev, S. V. Stepantsov, G. M. Ter-Akopian *et al.*, *Phys. Lett. B* **588**, 163 (2004).

[2] L. V. Grigorenko, I. G. Mukha, C. Scheidenberger, and M. V. Zhukov, *Phys. Rev. C* **84**, 021303(R) (2011).
 [3] N. K. Timofeyuk, *Phys. Rev. C* **65**, 064306 (2002).
 [4] S. Aoyama and N. Itagaki, *Phys. Rev. C* **80**, 021304(R) (2009).
 [5] D. Aleksandrov, Yu. A. Glukhov, A. S. Demyanova, V. I. Dukhanov, I. B. Mazurov, B. G. Novatsky, A. A. Ogloblin, S. B. Sakuta, and D. N. Stepanov, *Yad. Fiz.* **36**, 1351 (1982) [*Sov. J. Nucl. Phys.* **36**, 783 (1982)].
 [6] M. Gornov, M. Ber, Y. Gurov, S. Lapushkin, P. Morokhov, V. Pechurov, N. Poroshin, V. Sandukovsky, M. Tel'kushev, and B. Chernyshev, *J. Exp. Theor. Phys. Lett.* **77**, 344 (2003).
 [7] A. A. Korshennikov, E. Y. Nikolskii, E. A. Kuzmin, A. Ozawa, K. Morimoto, F. Tokanai, R. Kanungo, I. Tanihata, N. K. Timofeyuk, M. S. Golovkov *et al.*, *Phys. Rev. Lett.* **90**, 082501 (2003).
 [8] M. Caamaño, D. Cortina-Gil, W. Mittig, H. Savajols, M. Chartier, C. E. Demonchy, B. Fernández, M. B. Gómez Hornillos, A. Gillibert, B. Jurado *et al.*, *Phys. Rev. Lett.* **99**, 062502 (2007).
 [9] E. Y. Nikolskii, A. A. Korshennikov, H. Otsu, H. Suzuki, K. Yoneda, H. Baba, K. Yamada, Y. Kondo, N. Aoi, A. Denikin *et al.*, *Phys. Rev. C* **81**, 064606 (2010).
 [10] A. S. Fomichev, L. V. Grigorenko, S. A. Krupko, S. V. Stepantsov, and G. M. Ter-Akopian, *Eur. Phys. J. A* **54**, 97 (2018).
 [11] G. Kaminski, B. Zalewski, S. Belogurov, A. Bezbakh, D. Biare, V. Chudoba, A. Fomichev, E. Gazeeva, M. Golovkov, A. Gorshkov *et al.*, *Nucl. Instrum. Methods Phys. Res. Sect. B* (2019).
 [12] FRESKO, <http://www.fresco.org.uk/index.htm>.
 [13] O. Nemets *et al.*, *Nucleonic Associations in Atomic Nuclei and Nuclear Reactions of Multi-Nucleon Transfer* (Naukova Dumka, Kiev, 1988), in Russian.
 [14] W. W. Daehnick, J. D. Childs, and Z. Vrcelj, *Phys. Rev. C* **21**, 2253 (1980).
 [15] D. Y. Pang, W. M. Dean, and A. M. Mukhamedzhanov, *Phys. Rev. C* **91**, 024611 (2015).
 [16] C. Perey and F. Perey, *At. Data Nucl. Data Tables* **13**, 293 (1974).
 [17] P. Sharov, L. Grigorenko, A. Ismailova, and M. Zhukov, *JETP Lett.* **110**, 5 (2019).
 [18] D. Tilley, J. Kelley, J. Godwin, D. Millener, J. Purcell, C. Sheu, and H. Weller, *Nucl. Phys.* **A745**, 155 (2004).
 [19] M. S. Golovkov, L. V. Grigorenko, A. S. Fomichev, S. A. Krupko, Y. T. Oganessian, A. M. Rodin, S. I. Sidorchuk, R. S. Slepnev, S. V. Stepantsov, G. M. Ter-Akopian *et al.*, *Phys. Rev. C* **72**, 064612 (2005).
 [20] K. Markenroth, M. Meister, B. Eberlein, D. Aleksandrov, T. Aumann, L. Axelsson, T. Baumann, M. Borge, L. Chulkov, W. Dostal *et al.*, *Nucl. Phys.* **A679**, 462 (2001).
 [21] M. Meister, K. Markenroth, D. Aleksandrov, T. Aumann, T. Baumann, M. Borge, L. Chulkov, D. Cortina-Gil, B. Eberlein, T. Elze *et al.*, *Nucl. Phys.* **A700**, 3 (2002).
 [22] M. S. Golovkov, L. V. Grigorenko, G. M. Ter-Akopian, A. S. Fomichev, Y. T. Oganessian, V. A. Gorshkov, S. A. Krupko, A. M. Rodin, S. I. Sidorchuk, R. S. Slepnev *et al.*, *Phys. Lett. B* **672**, 22 (2009).